Indonesian Journal of Chemical Research

http://ojs3.unpatti.ac.id/index.php/ijcr Indo. J. Chem. Res., 14 (1), 40-52, 2026

Synthesis and Characterization of Modified Chrysophyllum albidum Seed Sodium Alginate Copolymers for Methylene Blue Removal

Nathanael Yinka Ilesanmi[1*], Funmilola Yetunde Falope[2], Adeiza Emmanuel Samuel[3], Esther Ayodotun Ilesanmi[1], Bamitale Fabiyi[1], Edwin Andrew Ofudje[1]

[1]Department of Chemical Sciences, Mountain Top University, Ibafo Ogun State
[2]Department of Chemical Sciences, Bells University Ota, Ogun State
[3]Department of Chemistry, Federal University of Agriculture, Zuru, Kebbi State-Nigeria
[*]*Corresponding Author: inathanael@mtu.edu.ng*

Received: January 2026
Received in revised: April 2026
Accepted: May 2026
Available online: May 2026

Abstract

This study aimed to evaluate the methylene blue adsorption performance of sodium alginate-based copolymers synthesized from acid-treated and base-treated Chrysophyllum albidum seed. The copolymers were prepared through chemical pretreatment and copolymerization with sodium alginate, then characterized using Fourier transform infrared spectroscopy, X-ray diffraction, and scanning electron microscopy to assess functional groups, structural arrangement, and surface morphology. Batch adsorption experiments were conducted under varying pH, adsorbent dosage, temperature, and contact time, while the data were evaluated using Box Behnken optimization, Langmuir and Freundlich isotherm models, and pseudo-first-order and pseudo-second-order kinetic models. The base-treated copolymer showed superior adsorption performance, achieving 90.1% maximum methylene blue removal compared with 79.9% for the acid-treated copolymer. It also recorded higher Langmuir adsorption capacity, stronger adsorption intensity, and better surface accessibility. The optimum conditions were pH 10.45, dosage 0.58 g, temperature 36.77 °C, and contact time 174.47 min, with desirability of 1.000. The adsorption kinetics followed the pseudo-second order model. The results indicate that base-treated Chrysophyllum albidum seed sodium alginate copolymer is a promising low-cost adsorbent for methylene blue removal from wastewater.

Keywords: adsorption, Chrysophyllum albidum seed, copolymer, sodium alginate, Box Behnken

INTRODUCTION

The release of industrial dyes, such as methylene blue, from various industrial processes into water bodies poses significant environmental and health concerns (Khan, 2021). Methylene blue is commonly applied in textile, paper, and pharmaceutical firms, and its presence in water can negatively impact both aquatic life and human health (Abbasi et al., 2024). Conventional wastewater treatment techniques, including chemical precipitation, membrane filtration, and biological treatment, have technical limitations in effective remediation of methylene blue from effluent streams (Wu, Shi, Li, Cai, & Chen, 2022).

African star seed (*Chrysophyllum albidum*) is a tropical fruit-bearing tree native to various regions in Africa, including West Africa, Central Africa, and parts of East Africa (Oderinde, Ibikunle, Bakre, & Babarinde, 2023). The seeds of the African starfruit are often discarded as agricultural waste, despite their potential for various applications (Shuaib, Musah, & Mathew, 2024). Recent studies have highlighted the potential of African star seed as an origin of useful compounds, including oils, proteins, and carbohydrates, which have applications across multiple industries (Audu, Beetseh, Edward-Ekpu, & Ewuga, 2019). African star seed is a promising natural resource with strong potential for the creation of adsorbent media. The seed contains a variety of functional groups, such as hydroxyl, carboxyl, and amino groups, which can interact with pollutants like methylene blue (Abdel-Halim, Alanazi, & Al-Deyab, 2015; Oderinde et al., 2023). Furthermore, its porous structure and extensive surface area of the seed can contribute to its adsorption capacity (Ayeni, Makinde, & Adeyemo, 2024; Oyefeso et al., 2025). However, the inherent limitations of using raw African star seed, such as low adsorption capacity and poor mechanical stability, have prompted the need for further modifications, resulting in the creation of composite materials.

(Bettaieb, Khiari, Dufresne, Mhenni, & Belgacem, 2015; Ogbu, Etuk-Udo, Ugoh, S.M.C., & Odunsanya, 2024).

Sodium alginate is a natural polysaccharide derived from brown seaweed, which has been widely applied in sectors such as food, pharmaceutical, and biomedical industries (Ching, Bansal, & Bhandari, 2017). It exhibits several important properties, including biocompatibility, biodegradability, and the capacity to generate hydrogels, rendering it a suitable candidate for the creation of adsorbent materials (Soni & Ghosh, 2017). The incorporation of sodium alginate into adsorbent materials can enhance their performance and stability, leading to improved adsorption capacities and reusability (Soli, Jraba, & Elaloui, 2023). Sodium alginate has been thoroughly researched for its capability to adsorb a diverse array of pollutants, including heavy metals, dyes, and organic compounds (Aragaw & Bogale, 2021). The carboxyl and hydroxyl groups within the alginate structure enable interaction with contaminants via pathways such as ion exchange, complexation, and hydrogen bonding. Additionally, the hydrogel-forming ability of sodium alginate can be utilised to immobilise adsorbent materials and improve their stability and reusability (Akl, Mostafa, Al-Awadhi, Al-Harwi, & El-Zeny, 2023; Oyefeso et al., 2025).

Multiple studies have documented the practice of copolymers synthesised from natural materials and biopolymers for the extraction of various pollutants, including methylene blue (Ali, 2019). These copolymers have shown enhanced adsorption capacities, selectivity, and regeneration capabilities compared to their individual components (Okoye-Anigbogu, Nwaokoro, Nwagbara, & Onuegbu, 2025). The optimisation of the copolymerization process and the assessment of the adsorption performance under different operating conditions are crucial steps in developing effective adsorbent materials for water quality improvement (Berradi, Aziz, Achaby, Ouazzani, & Mandi, 2023; Taba & Hala, 2021). This research contributes to the development of sustainable, eco-friendly adsorbent materials for the extraction of methylene blue from wastewater. The utilisation of African star seed, an underutilised agricultural waste, in the preparation of copolymers with sodium alginate can provide a cost-effective and environmentally friendly solution for water treatment (Guo, Qin, Chang, & Lee, 2023). The comprehensive evaluation of the adsorption performance, including the optimization of operating conditions using the Box–Behnken experimental design, can enable the identification of one of the most effective copolymer formulations for practical applications (Radoor et al., 2024).

Although several studies have investigated alginate and biomass adsorbents separately, limited information is available on copolymers prepared from modified *Chrysophyllum albidum* seed and sodium alginate for methylene blue removal. The novelty of this study is the use of acid-treated and base-treated African star apple seeds incorporated with sodium alginate and the comparison of their adsorption behaviour using response surface methodology, isotherm analysis, and kinetic modelling. Therefore, this research aimed to synthesize and characterize modified African star apple seed sodium alginate copolymers and evaluate their efficiency, optimum adsorption conditions, isotherm behaviour, and kinetic mechanism for methylene blue sorption from aqueous solution.

METHODOLOGY

Materials and Instrumentals

Chemicals used in this study included African star apple (*Chrysophyllum albidum*) seeds collected from local farms, distilled water, Hydrochloric acid (HCl, 37%, Merck, Darmstadt, Germany), sodium hydroxide (NaOH, ≥99%, Merck, Darmstadt, Germany), glacial acetic acid (≥99.8%, Sigma-Aldrich, St. Louis, MO, USA), methylene blue (molecular weight = 319.85 g/mol, ≥98%, Sigma-Aldrich, St. Louis, MO, USA), acetone (HPLC grade, ≥99.9%, Merck, Darmstadt, Germany and Sodium Alginate (analytical grade, Sigma-Aldrich, St. Louis, MO, USA) were used as received without further purification. Distilled water was used for all solution preparations and washing procedures.

The instruments and equipment used in this study included a hot air oven, laboratory milling machine, 100 µm sieve, magnetic stirrer, filtration apparatus, and volumetric glassware. Surface morphology analysis was carried out using scanning electron microscopy (SEM; Prisma E, Thermo Fisher Scientific, USA). Fourier-transform infrared (FTIR) spectra were recorded using an FTIR spectrometer manufactured by Agilent Technologies, while X-ray diffraction (XRD) analysis was performed using an X-ray diffractometer manufactured by Rigaku, Japan. Experimental design and statistical optimization were conducted using Design-Expert software version 13.0.0 developed by Stat-Ease Inc., Minneapolis, MN, USA.

Methods

Collection and Pretreatment of African star seeds

Seeds of African star apple (*Chrysophyllum albidum*) were sourced from local farms. The collected seeds were thoroughly rinsed with distilled water to eliminate surface impurities, then dried in a hot air oven at 105 °C. After drying, the seeds were ground into fine powder using a laboratory milling machine and passed through a 100 µm sieve. The processed powder was stored in polyethylene bags and kept in a dry environment until further use.

Acid Treatment of African star seed powder

A 5.0 g portion of the seed powder was treated with 0.1 M hydrochloric acid (HCl) using a solid-to-liquid ratio of 1:10 (w/v) in a 500 mL flask. The mixture was stirred using a magnetic stirrer at 200 rpm for 2 hours at 60 °C, after which it was left undisturbed at room temperature for 24 hours. The treated sample was then filtered and repeatedly washed with distilled water until a neutral pH (litmus test) was achieved. The material was subsequently dried in an oven at 105 °C. (Samuel, Kamba, Samaila, & Ilesanmi, 2024).

Mercerisation of African star (Chrysophyllum albidum) seed powder

For alkaline treatment, 5.0 g of the seed powder was mixed with 100 mL of 0.1 M sodium hydroxide (NaOH). The suspension was stirred at 200 rpm for 2 hours at 60 °C and then allowed to stand for 24 hours at room temperature. The treated sample was filtered, thoroughly rinsed with distilled water until neutral to litmus, and dried in a hot air oven at 105 °C.

Copolymerization of Acid and Base-Treated Africa Star Seed with Sodium Alginate

Copolymer formation was carried out by dissolving 5.0 g of the acid-treated seed powder in a 3% acid solution. The mixture was stirred at 200 rpm for 4 hours at 70 °C. Separately, 5.0 g of sodium alginate was dissolved in 50 mL of distilled water, and this solution was gradually added to the prepared mixture in a 500 mL volumetric flask. The resulting blend was stirred continuously for 2 hours at 40 °C. The formed copolymer was precipitated using acetone, then dried in an oven at 105 °C and stored in an airtight container for further characterization and adsorption analysis. The same procedure was repeated for the base-treated sample to obtain copolymer B.

Characterisation of the adsorbent

The surface morphology of the prepared copolymer samples was examined using scanning electron microscopy (SEM; Prisma E, Thermo Fisher Scientific, USA) operated at an accelerating voltage of 20 kV. The working distance was maintained at approximately 11.3 mm under low vacuum conditions. Samples were analysed directly without conductive coating. Fourier-transform infrared (FTIR) spectra were recorded using an Agilent Technologies FTIR spectrometer in transmittance mode over a wavenumber range of 4000–650 cm^{-1}. Spectra were acquired at a resolution of 8 cm^{-1} with 32 scans per sample and 16 background scans using Happ–Genzel apodization. X-ray diffraction (XRD) patterns were obtained using an X-ray diffractometer (Rigaku, Japan) equipped with Cu Kα radiation (λ = 1.5406 Å). Measurements were carried out over a 2θ range of 3°–70° with a step size of 0.02° and a scan step time of 1 s under ambient conditions. These analytical techniques were employed to evaluate the structural, functional group characteristics, and surface morphology of the synthesised copolymer.

Batch Adsorption Experiments using Box-Behnken Design

Response surface methodology (RSM) based on the Box-Behnken design (BBD) was employed to investigate the effects of four independent variables on methylene blue removal efficiency: adsorbent dosage (A), pH (B), contact time (C), and temperature (D), as shown in Table 1. BBD was selected because it enables efficient evaluation of the main, quadratic, and interaction effects of multiple variables while requiring fewer experimental runs than a full factorial design. Each factor was studied at three coded levels (-1, 0, and +1). The initial concentration of methylene blue used was 50 ppm. A total of 29 experimental runs were generated for each copolymer using Design-Expert software (version 13.0.0, Stat-Ease Inc., Minneapolis, MN, USA). The chosen experimental ranges were selected from relevant literature on methylene blue adsorption in related biopolymer systems and from practical operating limits suitable for the synthesised adsorbents (Halici & Demirhan, 2025).

Table 1. Box Behnken design variables and levels

Factor	Variable	Unit	Low level	Centre level	High level
A	pH	None	3	7	13
B	Adsorbent dosage	g	0.2	0.6	1
C	Temperature	°C	25	42.5	60
D	Contact time	min	30	105	180

Data Analysis

At the end of each experiment, the solutions were filtered, and the residual methylene blue concentration in the filtrate was determined using a UV-visible spectrophotometer at a wavelength of 664 nm. The methylene blue removal efficiency (R, %) was calculated using the following equation:

$$R\ (\%) = [(C_0 - C^t) / C_0] \times 100 \quad (1)$$

Where:

C_0 is the initial methylene blue concentration (mg/L)

C_t is the methylene blue concentration at time t (mg/L)

The experimental data obtained from the Box-Behnken design were analysed using statistical software to develop mathematical models and optimize the adsorption process parameters.

Adsorption isotherm and kinetic studies

A vital concept that describes the relationship between the concentration at equilibrium and the amount of dye adsorbed is the adsorption isotherm. Models such as the Langmuir and the Freundlich models were chosen to analyse the methylene adsorption experiment data.

Langmuir model

The Langmuir model is used to define that the adsorption occurs in a single layer on the adsorbent's surface, and no additional adsorption occurs after that.

$$\frac{C_e}{q_e} = \frac{1}{q_{max} \times K_L} + \frac{1}{q_{max}} C_e \quad (2)$$

Where,

C_e = equilibrium concentration of adsorbate in the solution (mg/L)

q_e = amount of adsorbate adsorbed at equilibrium per unit mass of adsorbent (mg/g)

q_{max} = maximum monolayer adsorption capacity of the adsorbent (mg/g)

K_L = Langmuir constant related to the affinity or adsorption energy (L/mg)

Freundlich model

The multilayer adsorption on a heterogeneous surface with an inconsistent, nonuniform distribution of energy and active sites is described by the Freundlich model.

$$\ln q_e = ln\ K_F + \frac{1}{n}\ lnC_e \quad (3)$$

Where K_F and n are coefficients that indicate the adsorption capacity and adsorption intensity, respectively. Adsorption kinetics is used to explain the mechanism of the adsorption processes and adsorption behaviour. Among the several methodologies accessible for analysis of adsorption mechanism, two kinetic models, the pseudo-first order model (Eq. 4) and the pseudo-second order model (Eq. 5), were used to assess the data from the adsorption process as follows:

Pseudo first-order kinetic model

$$\log(q_e - q_t) = \log q_e - \frac{k_1 t}{2.303} \quad (4)$$

Where K_1 (min^{-1}) is the rate constant, qt (mg/g) is the adsorbed amount at time.

Pseudo-second-order kinetic model

The pseudo-second-order model is given by:

$$\frac{1}{q_t} = \frac{1}{k_2 q_e^2} + \frac{t}{q_e} \quad (5)$$

Where k_2 (g/mg·min) denotes the rate constant of the pseudo-second-order model (Zhao et al., 2023).

RESULTS AND DISCUSSION

FT-IR Spectra for the Copolymers

The FTIR spectra of Copolymer A (acid-treated African star seed + sodium alginate) and Copolymer B (base-treated African star seed + sodium alginate), as shown in Figure 1, confirm successful copolymer formation. Both spectra exhibit a broad O–H stretching band around 3330 cm^{-1}, indicating hydroxyl groups from polysaccharides, and a C–H stretch near 2920 cm^{-1}, characteristic of aliphatic chains. Copolymer A shows a pronounced C=O stretching at 1735 cm^{-1}, suggesting protonated carbonyl or ester groups introduced by acid activation. In contrast, Copolymer B displays a weaker carbonyl band but stronger $–COO^–$ asymmetric and symmetric stretching near 1620 cm^{-1} and 1410 cm^{-1}, reflecting formation of sodium carboxylates due to alkaline hydrolysis. The C–O–C and C–O vibrations within 1020–1080 cm^{-1} confirm preservation of the alginate backbone (Li et al., 2024).

These spectral differences imply that acid treatment enhanced protonated functional groups favourable for hydrogen bonding, whereas base treatment increased deprotonated carboxylate sites, enhancing electrostatic interaction with cationic methylene blue molecules. Therefore, Copolymer B is expected to exhibit higher adsorption affinity. Similar functional modifications have been reported for alginate-based biosorbents (Chen et al., 2022).

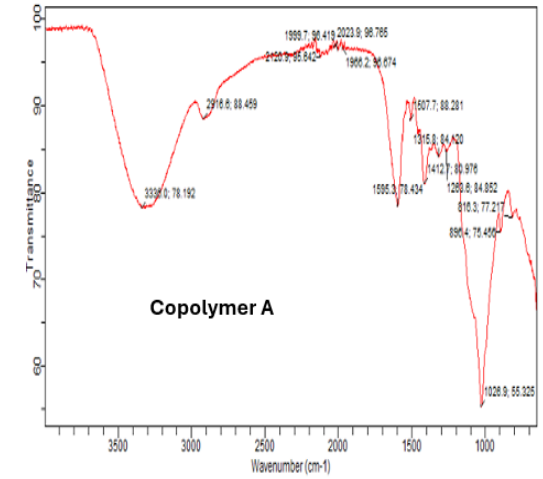

(a)

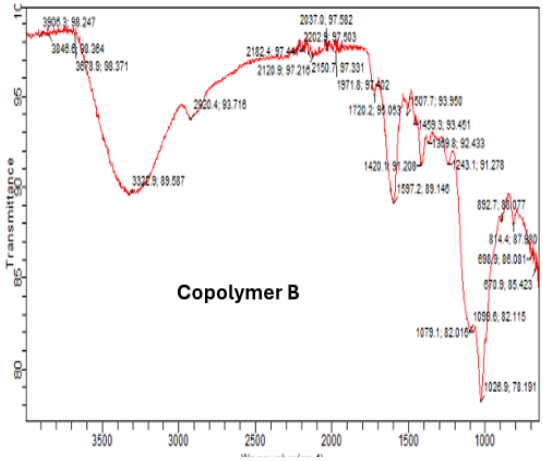

(b)

Figure 1. FTIR spectra of (a) Copolymer A and (b) Copolymer B

XRD Analysis for the Copolymers

The X-ray diffraction patterns of Copolymer A and Copolymer B in Figure 2 show that both materials possess semi-crystalline characteristics. The diffractograms contain broad diffraction regions together with some sharper peaks, indicating the coexistence of amorphous and crystalline phases. The XRD profiles of the two copolymers are generally similar, showing that acid and base treatment did not completely alter the main structural framework of the *Chrysophyllum albidum* seed-based copolymers. However, slight differences in peak intensity and broadness can be observed. Copolymer A showed somewhat sharper and more defined peaks, suggesting a relatively more ordered structure. This may be linked to acid treatment, which can remove some amorphous impurities and expose more ordered cellulose-rich regions. Such structural ordering may contribute to better material stability during adsorption (Arisa, Wirawan, & Widodo, 2025; Grigoraș & Simion, 2024).

In comparison, Copolymer B showed a broader diffraction background, suggesting a slightly more amorphous structure. This may be due to the effect of alkaline treatment, which can cause swelling of the biomass structure, disruption of hydrogen bonding, and loosening of polymer chains. Although the difference between the XRD patterns is not very large, the slightly more amorphous nature of Copolymer B may improve surface accessibility and facilitate diffusion of methylene blue molecules into the adsorbent matrix.

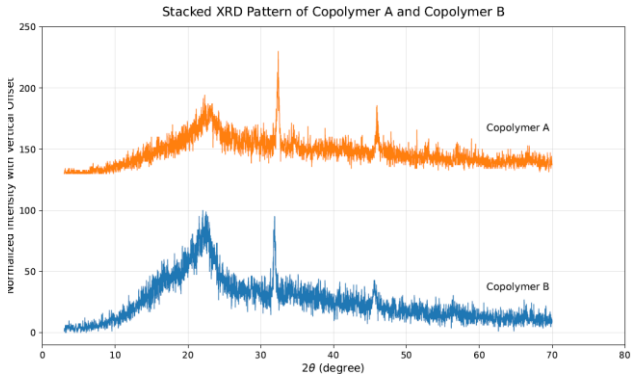

Figure 2. XRD pattern for Copolymer A and B

SEM Analysis for the Copolymers

The morphology of the copolymers was presented in Figure 3. The micrographs reveal a striking difference in morphology between Copolymer A and Copolymer B. The image of Copolymer A shows relatively smooth, large-scale folded or lamellar structures, indicative of a continuous, compact polymer matrix with minimal surface porosity. In contrast, Copolymer B exhibits a rough, granular "cauliflower-like" surface made up of sub-micron to micron-scale nodules and voids consistent with a highly porous or phase-separated topology rather than a homogeneous matrix (Tuzen, Sarı, & Saleh, 2018).

This contrast suggests that Copolymer A likely exhibits stronger chain packing, better miscibility, or stronger intermolecular cohesion, resulting in a denser morphology. Copolymer B, however, may involve phase separation, porogen-induced porosity, or rapid solvent evaporation/phase demixing during processing, leading to a porous particulate network. Such porous morphologies often lead to higher specific surface area and altered transport or interfacial properties (Priyanto, F., Muhdarina, & A., 2021).

Comparing these findings to existing literature, many studies on porous copolymer systems report similar granular or nodular SEM textures when porogens or nonsolvent-induced phase separation are

used. For example, in the review of porous copolymer resins, varying solvent/porogen ratios produced tunable pore structures with morphologies ranging from microporous networks to macroporous, granular surfaces (Zhao et al., 2023). Meanwhile, continuous dense morphologies akin to what is seen for Copolymer A are typical of well-compatibilized or well-crystallized polymer films or blends. Thus, the morphology observed in Copolymer B aligns with literature reports of intentionally porous or phase-separated copolymer systems, while Copolymer A corresponds to dense, well-packed polymer matrices.

The SEM morphology also agrees with the XRD interpretation. Copolymer A appears rough but more compact, with folded and aggregated surface features. This compact structure may explain its more crystalline behaviour in the XRD pattern. Such a surface can still adsorb methylene blue, but dye movement into deeper internal sites may be relatively limited. Copolymer B shows a rougher, more irregular, and more porous morphology. This type of surface is more favourable for adsorption because it provides more contact points for methylene blue molecules and allows easier penetration into the adsorbent matrix. Therefore, the SEM result supports the idea that Copolymer B has better surface accessibility than Copolymer A.

It should be noted that FTIR, XRD, and SEM analyses in this study were used to evaluate the functional groups, structural arrangement, and surface morphology of the prepared copolymers before adsorption. Therefore, these characterisation results are discussed as supporting evidence for the adsorption potential of the materials. The adsorption behaviour and possible uptake mechanism were further interpreted using the isotherm, kinetic, and optimisation results.

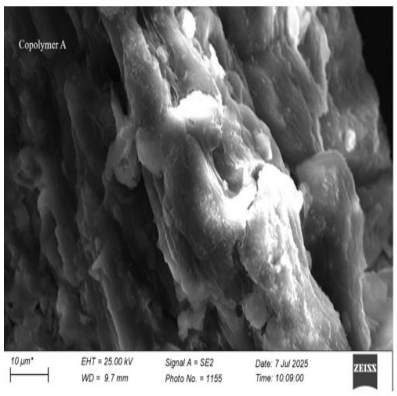

(a)

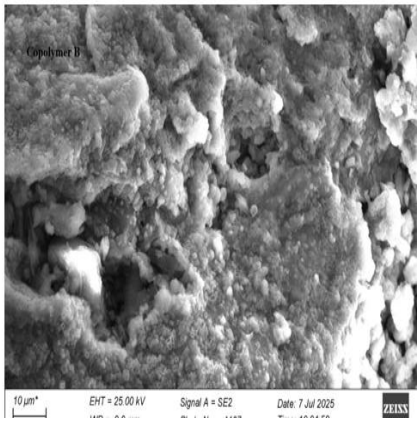

(b)

Figure 3. SEM morphology for (a) Copolymer A and (b) Copolymer B

The Predicted vs. Actual Plots for the Copolymers

Figure 4 presents the predicted versus Actual plots for Copolymer A and Copolymer B, which evaluate the adequacy and accuracy of the developed adsorption models. For an ideal model, all data points should lie close to the 45° line, indicating a perfect correlation between the predicted and experimental (actual) values (Tuzen et al., 2018). In the case of Copolymer A, most of the data points are closely aligned along the diagonal line, indicating strong agreement between predicted and actual values. This suggests that the developed regression or RSM model provides a reliable prediction of adsorption efficiency, with minimal deviation. The uniform distribution of the data points also indicates good homoscedasticity and absence of systematic error in the model. Conversely, Copolymer B shows a slightly wider scatter around the line of equality, particularly at higher and lower adsorption values. This dispersion implies a moderate deviation between experimental and predicted data, suggesting that the model fits Copolymer B data less precisely compared to Copolymer A. The variation may be attributed to the higher structural heterogeneity and amorphous nature of the base-treated copolymer, as observed from its XRD profile.

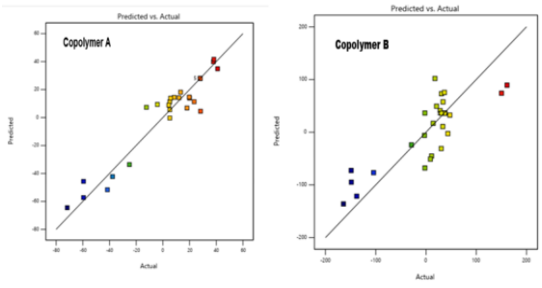

Figure 4. Predicted vs actual value for Copolymer A and Copolymer B

The 3D surface interaction response between Contact Time and Adsorbent Dosage

The 3D surface plots in Figure 5 illustrate the interactive effects of adsorbent dosage and contact time on the percentage removal of the methylene blue by Copolymer A and Copolymer B. Both copolymers displayed positive correlations between contact time and removal efficiency, consistent with the expected adsorption behaviour in which increased interaction time enhances solute diffusion to active binding sites (Ogundiran, Ofudje, Ogundiran, & Adewusi, 2022). For Copolymer A, the response surface is smoother and more elevated, indicating that percentage removal increases steadily with both contact time and dosage. The steep gradient observed suggests that both variables significantly influence adsorption efficiency. The improvement in removal with higher dosage can be attributed to the increased availability of active sites, while prolonged contact time allows equilibrium to be reached (Abbasi et al., 2024). The red region at the surface apex represents optimal adsorption, suggesting a favourable kinetic response and strong adsorbent–adsorbate interaction, consistent with its higher crystallinity observed in the XRD analysis. In contrast, Copolymer B shows a relatively flatter surface, implying a less pronounced effect of time and dosage. The moderate slope suggests that while removal efficiency increases slightly with dosage and time, the response is less sensitive compared to Copolymer A. This behaviour can be linked to the more amorphous structure of Copolymer B, which, though porous, may exhibit less uniform adsorption site distribution (Zhao et al., 2023).

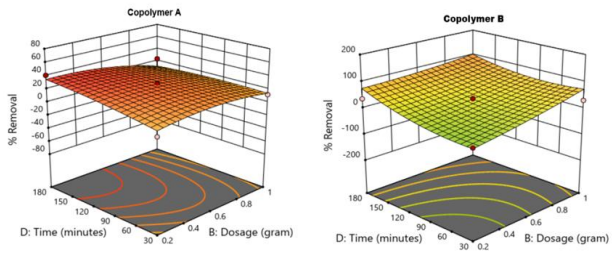

Figure 5. The 3D surface interaction response between adsorbent dosage and contact time

The 3D surface interaction response between Adsorbent Dosage and pH

The 3D surface plots in Figure 6 depict the combined effects of solution pH and adsorbent dosage on the percentage removal of methylene blue for Copolymer A and Copolymer B. These parameters significantly affect adsorption because they determine both the surface charge of the adsorbent and the degree of ionization of the adsorbate species (Tuzen et al., 2018). For Copolymer A, the surface plot shows a steady increase in percentage removal with increasing dosage and moderate pH. The response surface is relatively steep, suggesting that dosage exerts a stronger influence than pH. This trend may be attributed to the higher number of available binding sites at larger dosages, which enhances adsorption efficiency. The moderate optimum observed around pH 6–8 can be linked to a balanced electrostatic attraction between the functional groups on the copolymer (–OH, –COOH) and the ionic adsorbate species. At lower pH values, protonation of active sites likely reduces adsorption efficiency (Ogundiran et al., 2022). In contrast, Copolymer B demonstrates a more curved surface, indicating that both pH and dosage strongly influence adsorption. The removal efficiency rises significantly at higher pH values, suggesting that deprotonation of the copolymer surface enhances electrostatic attraction toward cationic species. This behaviour aligns with the more amorphous and porous nature of Copolymer B, as revealed by XRD analysis, which allows for greater interaction with adsorbate molecules under favourable pH conditions (Ogundiran et al., 2022). Overall, Copolymer A performs optimally at moderate pH and higher dosages, while Copolymer B shows improved adsorption at higher pH due to increased surface ionization and porosity. The interaction between pH and dosage is therefore crucial for optimizing adsorption efficiency in both copolymers.

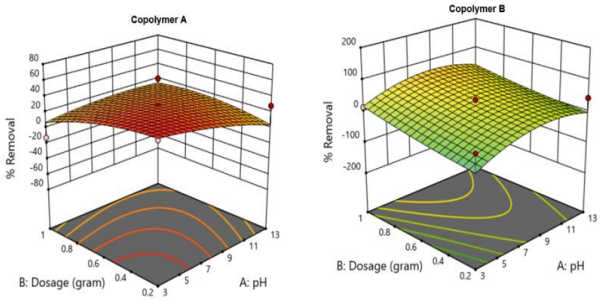

Figure 6. The 3D surface interaction response between adsorbent dosage and pH

The 3D surface interaction response between Temperature and Adsorbent Dosage

The interactive effect of temperature and adsorbent dosage, as shown in Figure 7, on the percentage removal efficiency of Copolymer A and Copolymer B. Both copolymers exhibited temperature-

dependent adsorption behaviour, suggesting that thermal energy influences the diffusion and binding of adsorbate molecules onto the copolymer surfaces. For Copolymer A, the surface plot demonstrates that adsorption efficiency increases initially with temperature and dosage, reaching an optimum within the range of 35–45 °C. Beyond this point, a slight decline in removal efficiency is observed, indicating that excessive temperature may disrupt adsorbate–adsorbent interactions or cause partial desorption. The increase in adsorption with temperature at moderate levels suggests that the process is endothermic, enhancing molecular mobility and facilitating active site accessibility (Kawhena, Opara, & Fawole, 2021). Similarly, higher dosage contributes to greater removal due to the availability of more active binding sites. In contrast, Copolymer B displays a more pronounced response to temperature changes, with removal efficiency improving substantially as both temperature and dosage increase. The steeper surface curvature indicates a stronger temperature dependence compared to Copolymer A. This trend implies that adsorption onto Copolymer B is also endothermic, but more diffusion-controlled due to its amorphous structure, as confirmed by XRD analysis. The enhanced performance at elevated temperatures can be attributed to increased pore diffusion and activation of binding sites (Abbasi et al., 2024; El-Rayyes et al., 2025). Overall, the response surfaces reveal that both copolymers exhibit endothermic adsorption behaviour, with Copolymer A showing moderate thermal sensitivity due to its higher crystallinity, while Copolymer B demonstrates a more temperature-driven adsorption response attributed to its higher porosity and flexibility.

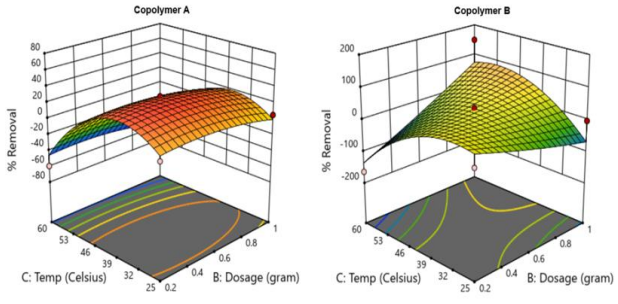

Figure 7. The 3D surface interaction response between temperature and adsorbent dosage

ANOVA and FIT Summary for the Copolymers.

The ANOVA results for the quadratic model describing methylene blue removal by Copolymers A and B are presented in Table 1a and 1b. The model for Copolymer A is statistically significant ($p < 0.0001$; $F = 11.49$), indicating that the quadratic model adequately represents the adsorption process. Among the individual parameters, temperature (C) exhibited the highest F-value (62.50) with a highly significant p-value ($p < 0.0001$), revealing that temperature is the most influential factor controlling the adsorption of methylene blue onto Copolymer A. The quadratic term of temperature (C^2) was also highly significant ($F = 80.79$, $p < 0.0001$), confirming that the effect of temperature on removal efficiency is nonlinear. Conversely, pH, dosage, and time contributed less significantly ($p > 0.05$), although pH ($p = 0.0653$) had a marginal influence. This outcome implies that temperature-driven activation of adsorption sites and increased diffusion rates are the dominant mechanisms, consistent with endothermic adsorption behaviour reported for polysaccharide-based composites (Samuel et al., 2024). For Copolymer B, the quadratic model was not statistically significant ($p = 0.0771$; $F = 2.19$), suggesting that the experimental data were not fully described by the quadratic equation. However, specific interaction terms such as BC (dosage × temperature) ($p = 0.0276$) and CD (temperature × time) ($p = 0.0237$) were significant, indicating that the removal efficiency depends strongly on the combined effects of process variables rather than on individual parameters. The significance of these interaction terms reflects the complex synergistic relationship between temperature and adsorbent dosage, where simultaneous increases can enhance adsorption due to improved molecular mobility and greater availability of active sites. The non-significance of the overall model for Copolymer B may result from a broader experimental variability or a more heterogeneous surface structure compared to Copolymer A, as reported by similar studies on biopolymer-based adsorbents (Kanani et al., 2022). The lack-of-fit for Copolymer A was not significant, confirming good model adequacy. However, Copolymer B showed a significant lack of fit ($p < 0.0001$), suggesting that additional model terms or alternative transformations might better capture the adsorption behaviour.

ANOVA and Model Adequacy

The ANOVA results for the copolymers are presented in Tables 2a and 2b. For Copolymer A, the model was statistically significant ($F = 11.49$; $p < 0.0001$), showing that the selected model adequately represented methylene blue removal. Temperature had the strongest individual effect on the response, and the quadratic temperature term was also significant,

confirming that temperature influenced adsorption in a nonlinear manner. For Copolymer B, the overall quadratic model was not significant at $p < 0.05$, while some interaction or quadratic terms were significant. This suggests that the response of Copolymer B was more interaction-dependent and less adequately described by the current quadratic model. The significant lack of fit for Copolymer B indicates that model transformation, additional experimental points, or alternative model terms may be required.

Table 2a. ANOVA and fit summary for Copolymer A

Source	Sum of squares	df	Mean square	F value	p value	Decision
Model	25019.61	14	1787.12	11.49	<0.0001	Significant
A: pH	621.94	1	621.94	4.00	0.0653	Not significant
B: dosage	404.38	1	404.38	2.60	0.1292	Not significant
C: temperature	9719.09	1	9719.09	62.50	<0.0001	Significant
D: time	249.52	1	249.52	1.60	0.2259	Not significant
AB	440.79	1	440.79	2.83	0.1144	Not significant
AC	271.92	1	271.92	1.75	0.2073	Not significant
AD	320.41	1	320.41	2.06	0.1731	Not significant
BC	0.0000	1	0.0000	0.0000	1.0000	Not significant
BD	143.16	1	143.16	0.9206	0.3536	Not significant
CD	0.0870	1	0.0870	0.0006	0.9815	Not significant
A^2	138.00	1	138.00	0.8874	0.3622	Not significant
B^2	318.63	1	318.63	2.05	0.1743	Not significant
C^2	12563.55	1	12563.55	80.79	<0.0001	Significant
D^2	39.29	1	39.29	0.2527	0.6230	Not significant
Residual	2177.23	14	155.52			
Lack of fit	2177.23	10	217.72			Not significant
Pure error	0.0000	4	0.0000			

Table 2b. ANOVA and fit summary for Copolymer B

Source	Sum of squares	df	Mean square	F value	p value	Decision
Model	115500.00	14	8248.38	2.19	0.0771	Not significant
A: pH	3333.00	1	3333.00	0.8857	0.3626	Not significant
B: dosage	8374.08	1	8374.08	2.23	0.1580	Not significant
C: temperature	698.60	1	698.60	0.1856	0.6731	Not significant
D: time	9145.88	1	9145.88	2.43	0.1414	Not significant
AB	85.91	1	85.91	0.0228	0.8820	Not significant
AC	1405.63	1	1405.63	0.3730	0.5512	Not significant
AD	69.33	1	69.33	0.0184	0.8939	Not significant
BC	24713.41	1	24713.41	6.57	0.0276	Significant
BD	693.31	1	693.31	0.1843	0.6742	Not significant
CD	24258.14	1	24258.14	6.45	0.0237	Significant
A^2	9658.51	1	9658.51	2.57	0.1315	Not significant
B^2	168.23	1	168.23	0.0447	0.8356	Not significant
C^2	27001.38	1	27001.38	7.18	0.0190	Significant
D^2	340.00	1	340.00	0.0912	0.4197	Not significant
Residual	52683.41	14	3763.13			
Lack of fit	52643.45	10	5264.35	526.36	<0.0001	Significant
Pure error	39.96	4	10.00			

Adsorption Isotherm Model

The isotherm parameters are presented in Table 3. Copolymer A was better described by the Langmuir model because its Langmuir coefficient of determination (R^2 = 0.974) was higher than the Freundlich value (R^2 = 0.901). This suggests that methylene blue uptake on Copolymer A was closer to monolayer adsorption on more uniform active sites. For Copolymer B, the Freundlich model showed a slightly higher R^2 value (0.9843) than the Langmuir model (0.973). Although the difference is not large, Freundlich was considered marginally more suitable for Copolymer B because the SEM morphology and interaction dominated RSM behaviour suggest a more heterogeneous surface. These findings align with FTIR-based surface chemistry: base treatment (Copolymer B) likely produces abundant deprotonated (anionic) carboxylate and hydroxyl groups, increasing negative surface charge and electrostatic attraction to the cationic methylene blue (Ikhsan, Sekewael, & Hasanela, 2022; Mohanty, Behera, & Patra, 2025). The revised wording, therefore, presents Freundlich as the better empirical fit rather than as absolute proof of the mechanism.

Table 3. Isotherm parameters for the Copolymers

Isotherm	Parameters	Copolymer A	Copolymer B
Langmuir	q_{max} (mg/g)	19.346	44.64
	RL	0.019	0.004
	KL	0.498	2.24
	R^2	0.974	0.973
Freundlich	K_F (mg/g)(mg/L)1/2	7.488	21.806
	N	0.584	1.711
	R^2	0.901	0.9843

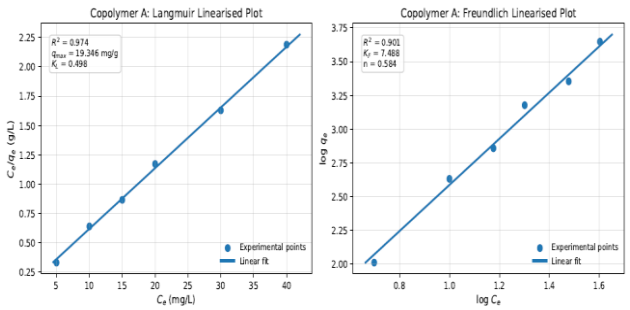

(a)

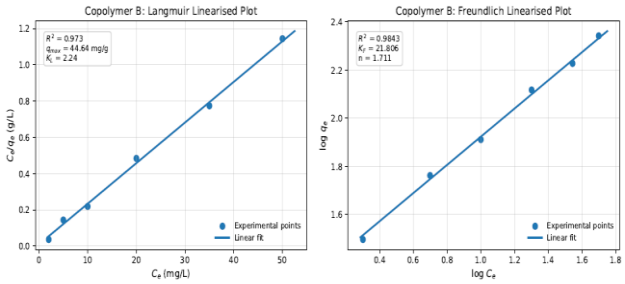

(b)

Figure 8. Isotherm plot for (a) Copolymer A and (b) Copolymer B

Adsorption Kinetic Studies

The adsorption kinetics parameters, as presented in Table 4 for both Copolymer A and B, showed that the copolymers were best described by the pseudo-second-order model (high R^2 = 0.99), consistent with most alginate and chitosan-based adsorbents. Chitosan-based adsorbents likewise fit PSO kinetics; for example, lignin-chitosan composites gave K1 10^{-3}–10^{-2} min^{-1}, K2 10^{-5}–10^{-3} $g \cdot mg^{-1} \cdot min^{-1}$ and q_e ≲30 mg/g in one study. pH-dependent pretreatments also markedly affect MB uptake: protonation of $–NH_2$ sites under acidic conditions generally enhances MB binding, whereas raising pH (deprotonating acidic groups) increases anionic sites for cationic MB (i.e., deprotonated $–COO^-$ groups) (Mohanty et al., 2025).

Table 4. Adsorption Kinetics Model for the Copolymers

Model	Parameters	Copolymer A	Copolymer B
Pseudo-first-order	Q_e(exp)	49.93	49.93
	Q_e(cal)	66.12	38.01
	K^1	0.035	0.012
	R^2	0.8044	0.957
Pseudo-second-order	Q_e(exp)	49.93	49.93
	Q_e(cal)	49.87	49.92
	K^2	0.0009	0.0004
	R^2	1	1

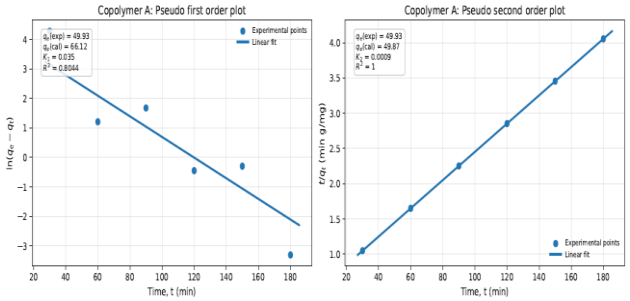

(a)

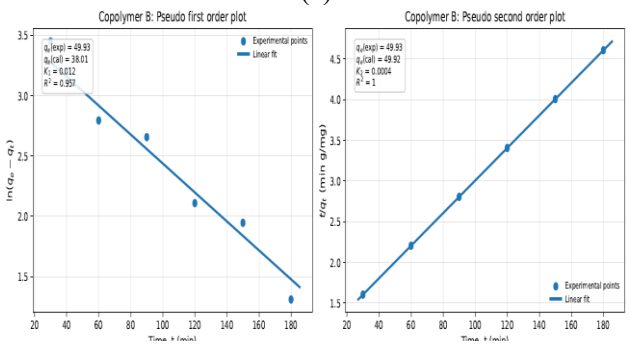

(b)

Figure 9. Adsorption kinetics odel for (a) Copolymer A and (b) Copolymer B

CONCLUSION

The study confirms that both acid-treated and base-treated C. albidum seed copolymers were effective for methylene blue removal, although the base-treated copolymer showed better adsorption performance. The XRD patterns showed only slight structural differences, suggesting that the improved performance was not due to crystallinity alone, but also to surface accessibility, morphology, and functional group exposure. The isotherm result supported this, as the base-treated copolymer recorded a higher Langmuir adsorption capacity of 44.64 mg/g compared with 19.346 mg/g for the acid-treated sample. The adsorption kinetics followed the pseudo-second order model, showing that uptake depended mainly on active adsorption sites. The optimisation study further predicted maximum methylene blue removal of 90.10 percent at pH 10.45, adsorbent dosage of 0.58 g, temperature of 36.77 °C, and contact time of 174.47 minutes, with desirability of 1.000. Overall, the base-treated copolymer is a promising adsorbent for methylene blue removal under optimized conditions.

REFERENCES

Abbasi, A., Ahmad, I., Abd El-Gawad, H. H., Alshahrani, W. A., Alqarni, N. D., El-Bahy, Z. M., & Ikram, S. (2024). Appraisal of the adsorption potential of novel modified gellan gum nanocomposite for the confiscation of methylene blue and malachite green. *International Journal of Biological Macromolecules*, *259*, 129221.

Abdel-Halim, E. S., Alanazi, H. H., & Al-Deyab, S. S. (2015). Utilization of olive tree branch cellulose in synthesis of hydroxypropyl carboxymethyl cellulose. *Carbohydrate Polymers*, *127*, 124–134.

Akl, M. A., Mostafa, A. G., Al-Awadhi, M., Al-Harwi, W. S., & El-Zeny, A. S. (2023). Zinc chloride activated carbon derived from date pits for efficient biosorption of brilliant green: Adsorption characteristics and mechanism study. *Applied Water Science*, *13*(12), 226.

Ali, A. H. (2019). Treatment of wastewater contaminated with dyes using modified low-cost adsorbents. *Desalination and Water Treatment*, *140*, 326–336.

Aragaw, T. A., & Bogale, F. M. (2021). Biomass-Based Adsorbents for Removal of Dyes From Wastewater: A Review. *Frontiers in Environmental Science*, *9*.

Arisa, P., Wirawan, T., & Widodo, N. T. (2025). Adsorption of Methylene Blue Using Composite Fe3O4-Ihau Fruit Peel Powder (Dimocarpus longan var. Malesianus Leenh.). *Indonesian Journal of Chemical Research*, *13*(2), 102–110.

Audu, S. S., Beetseh, C. I., Edward-Ekpu, D. U., & Ewuga, A. A. (2019). Proximate, Mineral Contents, and Physicochemical Properties of *Chrysophyllum Albidum* (African Star Apple) Kernel Flour and Oil. *Journal of Applied Sciences and Environmental Management*, *23*(7), 1245.

Ayeni, P., Makinde, F. M., & Adeyemo, F. O. (2024, September 21). *Phytochemical and in Vitro Antioxidant Potential of African Star Apple (Chrysophyllum Albidum) Components* [SSRN Scholarly Paper]. Rochester, NY: Social Science Research Network.

Berradi, A., Aziz, F., Achaby, M. E., Ouazzani, N., & Mandi, L. (2023). A Comprehensive Review of Polysaccharide-Based Hydrogels as Promising Biomaterials. *Polymers*, *15*(13), 2908.

Bettaieb, F., Khiari, R., Dufresne, A., Mhenni, M. F., & Belgacem, M. N. (2015). Mechanical and thermal properties of Posidonia oceanica cellulose nanocrystal reinforced polymer. *Carbohydrate Polymers*, *123*, 99–104.

Chen, T., Liu, H., Gao, J., Hu, G., Zhao, Y., Tang, X., & Han, X. (2022). Efficient Removal of Methylene Blue by Bio-Based Sodium Alginate/Lignin Composite Hydrogel Beads. *Polymers*, *14*(14), 2917.

Ching, S. H., Bansal, N., & Bhandari, B. (2017). Alginate gel particles-A review of production techniques and physical properties. *Critical Reviews in Food Science and Nutrition*, *57*(6), 1133–1152.

El-Rayyes, A., Ofudje, E. A., Bamgbade, A. A., Refat, M. S., Alsuhaibani, A. M., Akande, J. A., … Ilesanmi, N. Y. (2025). Malachite Green Adsorption by Base-treated Wood Mill Residues: Kinetics, Isotherms, and Thermodynamic Studies. *BioResources*, *20*(3), 7378–7404.

Grigoraș, C.-G., & Simion, A.-I. (2024). Synthesis of a New Composite Material Derived from Cherry Stones and Sodium Alginate—Application to the Adsorption of Methylene Blue from Aqueous Solution: Process Parameter Optimization, Kinetic Study, Equilibrium Isotherms, and Reusability. *Journal of Composites Science*, *8*(10), 402.

Guo, H., Qin, Q., Chang, J.-S., & Lee, D.-J. (2023). Modified alginate materials for wastewater treatment: Application prospects. *Bioresource Technology*, *387*(129639).

Halici, Z., & Demirhan, E. (2025). Response surface methodology for optimizing adsorption process parameters for tadalafil removal by raw eggshell. *Biomass Conversion and Biorefinery*, *15*(4), 6027–6036.

Ikhsan, N., Sekewael, S. J., & Hasanela, N. (2022). Kinetics and Isotherm Study of Ion Phosphate Adsorption by Lontor Natural Clay. *Indonesian Journal of Chemical Research*, *9*(3), 171–178.

Kanani, M., Kanani, N., Batooie, N., Bozorgian, A., Barghi, A., & Rezania, S. (2022). Removal of Rhodamine 6G dye using one-pot synthesis of magnetic manganese graphene oxide: Optimization by response surface methodology. *Environmental Nanotechnology, Monitoring & Management*, *18*, 100709.

Kawhena, T. G., Opara, U. L., & Fawole, O. A. (2021). Optimization of Gum Arabic and Starch-Based Edible Coatings with Lemongrass Oil Using Response Surface Methodology for Improving Postharvest Quality of Whole "Wonderful" Pomegranate Fruit. *Coatings*, *11*(4), 442.

Khan, S. H. (2021). Advanced approaches for heavy metals removal from industrial wastewater. In *New Trends in Removal of Heavy Metals from Industrial Wastewater* (pp. 403–440). Elsevier.

Li, W., Guo, M., Wang, Y., Deng, H., Lei, H., Yu, C., & Liu, Z. (2024). Selective adsorption of heavy metal ions by different composite-modified semi-carbonized fibers. *Separation and Purification Technology*, *328*, 125022.

Mohanty, N., Behera, S., & Patra, B. N. (2025). Fabrication of Fe_3O_4 /Polypyrrole/Phytic Acid Magnetic Nanocomposite for Preferential Adsorption of Cationic Dye: Adsorption Properties, Kinetics, and Mechanism. *Industrial & Engineering Chemistry Research*, *64*(4), 2274–2282.

Oderinde, A., Ibikunle, A., Bakre, L., & Babarinde, N. (2023). Effects of Acetylation, Acid-thinning and Oxidation on Chrysophyllum albidum (African Star Apple) Kernel Native Starch. *Chemical Papers*, *77*(9), 5385–5394.

Ogbu, J. C., Etuk-Udo, G., Ugoh, S. C., S.M.C., U., & Odunsanya, O. O. (2024, October 29). *Proximate and Mineral Content Analysis of African Star Apple (Chrysophyllum albidum)*. In Review.

Ogundiran, A. A., Ofudje, E. A., Ogundiran, O. O., & Adewusi, A. M. (2022). Cationic dye adsorptions by eggshell waste: Kinetics, isotherms, and thermodynamics studies. *Desalination and Water Treatment*, *280*, 157–167.

Okoye-Anigbogu, S., Nwaokoro, A.-P., Nwagbara, N., & Onuegbu, T. U. (2025). Chrysophyllum albidum Seed Shell-derived Activated Carbon: A Novel Adsorbent for Basic Red 9 (BR9) Dye Adsorption. *Journal of Applied Chemical Science International*, *16*, 157–174.

Oyefeso, B., Akwunwa, I., Ajayi, P., Akintola, A., Fadele, O., & Clement, O. (2025). Development of Predictive Mass and Volume Models for African Star Apple Fruits. *African Journal of Agricultural Science and Food Research*, *19*, 342–352.

Priyanto, A., F., M., Muhdarina, M., & A., A. (2021). Adsorption and Characterization of Activated Sugarcane Bagasse Using Sodium Hydroxide.

Indonesian Journal of Chemical Research, *8*(3), 202–209.

Radoor, S., Karayil, J., Jayakumar, A., Kandel, D. R., Kim, J. T., Siengchin, S., & Lee, J. (2024). Recent advances in cellulose- and alginate-based hydrogels for water and wastewater treatment: A review. *Carbohydrate Polymers*, *323*(121339).

Samuel, A., Kamba, S., Samaila, D., & Ilesanmi, N. (2024). Preparation and Characterization of Periwinkle Shell Based Chitosan-Kenaf fibre Copolymer and its Derivatives for Selective Binding of Cu (II) and Zn (II) ions from Electroplating Effluent. *Journal of Applied Sciences and Environmental Management*, *28*, 853–863.

Shuaib, M. M., Musah, M., & Mathew, J. T. (2024). Preparation and Characterization of Activated Carbon from Africa Star Apple (*Chrysophyllum Albidum*) Seed Shell. *Fudma Journal of Sciences*, *8*(3), 194–199.

Soli, J., Jraba, A., & Elaloui, E. (2023). Control Synthesis of Metallic Gold Decorated ZnO Nanoparticles for Photocatalytic Degradation of Rhodamine B, Methylene Blue and Eriochrome Black T Dyes. *Chemistry Select*, *8*(39).

Soni, S. R., & Ghosh, A. (2017). Exploring pullulan-poly(vinyl alcohol) interpenetrating network microspheres as controlled release drug delivery device. *Carbohydrate Polymers*, *174*, 812–822.

Taba, P., & Hala, Y. (2021). *Adsorption of Tetracycline Hydrochloride from Solutions Using Mesoporous Silica, MCM-48*.

Tuzen, M., Sarı, A., & Saleh, T. A. (2018). Response surface optimization, kinetic and thermodynamic studies for effective removal of rhodamine B by magnetic AC/CeO2 nanocomposite. *Journal of Environmental Management*, *206*, 170–177.

Wu, S., Shi, W., Li, K., Cai, J., & Chen, L. (2022). Recent advances on sustainable bio-based materials for water treatment: Fabrication, modification and application. *Journal of Environmental Chemical Engineering*, *10*(6), 108921.

Zhao, W., Hao, C., Guo, Y., Shao, W., Tian, Y., & Zhao, P. (2023). Optimization of Adsorption Conditions Using Response Surface Methodology for Tetracycline Removal by MnFe2O4/Multi-Wall Carbon Nanotubes. *Water*, *15*(13), 2392.